Science Advances

AAAS

advances.sciencemag.org/cgi/content/full/2/3/e1501329/DC1

Supplementary Materials for

Quantitative determination of pairing interactions for high-temperature superconductivity in cuprates

Jin Mo Bok, Jong Ju Bae, Han-Yong Choi, Chandra M. Varma, Wentao Zhang, Junfeng He, Yuxiao Zhang, Li Yu, X. J. Zhou

Published 4 March 2016, *Sci. Adv.* **2**, e1501329 (2016)
DOI: 10.1126/sciadv.1501329

The PDF file includes:

SI. Extraction of Normal and Pairing Self-Energy from ARPES in the Superconducting State

SI.1 The Single-Particle Spectral Function

SI.2 Procedure for Extracting the Self-Energy

SII. Correction of Systematic Errors and Renormalization of the ARPES Data

SII.1 Limits of Validity of Results

SIII. Equations for the Self-Energy

SIII.1 Exact Representation of the Self-Energy

SIII.2 Familar Eliashberg Integral Equations for d-wave Superconductors

SIV Comparison of Theories with the Results from Experiments.

I. Extraction of Normal and Pairing Self-Energies from ARPES in the Superconducting State

For the physics of the ARPES process, we refer to excellent reviews [4,5]. ARPES measures, for a given flux of photons of energy ν incident on a sample, the intensity of photo-electrons of kinetic energy E_{kin} and chosen angles at the detector with respect to the crystalline axes. Using the energy and momentum conservation laws, the kinetic energy and the angles can be converted into the energy ω and the crystal momentum $\mathbf{k}$ of the one-particle state of the sample before the photo-excitation. For the purposes of this work, it is necessary to measure the ARPES intensity $I(\mathbf{k},\omega)$ at different $\mathbf{k}$ and ω of interest and temperature T from just above T_c to well below it, with an accuracy of better than about 2%. Fig. 1 and Fig. 2 for UD89 give an idea of the quality of the raw data. We show similar results for the OD82 sample in Fig. S1, which are of somewhat poorer quality than in Fig. 1, but quite adequate for extracting the self-energies to the accuracy necessary for our conclusions.

In this section, we first cast $I(\mathbf{k},\omega)$ in a form suitable for our analysis in **SI.1**, and then explain the procedure of extracting the normal and pairing self-energies from the data in **SI.2**. The results obtained depend on the accuracy and consistency of the experimental data, which are checked. One encounters the issues of signal to noise in the data as well as systematic errors due to both variation of photon flux and the small movements of sample with respect to the source of photons and the detector as a function of temperature. One also needs to renormalize the momentum distribution curve (MDC) in the superconducting state such that any slight misfits in the normal state do not affect the superconducting state fits. In other words one should make sure that the pairing self-energy and accompanying deviation of the normal self-energy from above T_c are extracted only from the difference between the MDC data between below and above T_c for the same cut and ω. We explain how we minimize and take into account the systematic errors and how to renormalize the superconducting state MDC data in **SII**.

SI.1 The Single-Particle Spectral Function

The ARPES intensity $I(\mathbf{k},\omega)$ for unit-incident flux of photons is given, in the sudden approximation, by

$$I(\mathbf{k},\omega) = |M(\mathbf{k},\nu)|^2 f(\omega)[A(\mathbf{k},\omega) + B(\mathbf{k},\omega)] \tag{S1}$$

$M(\mathbf{k},\nu)$ is the matrix element of the photo-emission process, $f(\omega)$ the Fermi distribution function, and $B(\mathbf{k},\omega)$ is the background from the multiple scatterings of the photo-electrons, which in well done laser based ARPES is small and well characterized in MDC measurements as seen in Fig. 2. $A(\mathbf{k},\omega)$ is the single-particle spectral function given by the imaginary part of the retarded Green's function. Our primary interest is to extract the normal self-energy $\Sigma(\mathbf{k},\omega)$ and the pairing self-energy $\phi(\mathbf{k},\omega)$ in terms of which the Green's function is written.

$$A(\mathbf{k},\omega) = -\frac{1}{\pi} Im G_{11}(\mathbf{k},\omega) \tag{S2}$$

$$\hat{G}(\mathbf{k},\omega) = \frac{W(\mathbf{k},\omega)\tau_0 + Y(\mathbf{k},\omega)\tau_3 + \phi(\mathbf{k},\omega)\tau_1}{W^2(\mathbf{k},\omega) - Y^2(\mathbf{k},\omega) - \phi^2(\mathbf{k},\omega)} \tag{S3}$$

where the subscript in Eq. (S2) represents the 11 component of the matrix Green's function $\hat{G}$, and the τ_i $(i = 0,1,2,3)$ are the Pauli matrices in the Nambu space. As verified in Fig. 2, the normal self-energy and pairing self-energy depend on $k_\perp$ very weakly, and are functions of θ and ω. Then

$$W(\theta,\omega) = \omega - \Sigma_0(\theta,\omega) \equiv \omega Z(\theta,\omega) \tag{S4}$$

$$Y(\mathbf{k},\omega) = \xi(\mathbf{k}) + \Sigma_3(\theta,\omega) \tag{S5}$$

$$\phi(\theta,\omega) = Z(\theta,\omega)\Delta(\theta,\omega) \tag{S6}$$

The $\Sigma_3(\theta,\omega)$ is in principle necessary because we need to consider self-energies over a large energy region from the chemical potential, where $\xi(\mathbf{k})$ is not symmetric, and the impurity induced resonance[10,11] in the superconducting state come from potentials which are in general not particle-hole symmetric. The normal self-energy $\Sigma(\theta,\omega)$ is given by

$$\Sigma(\theta,\omega) = \Sigma_0(\theta,\omega) + \Sigma_3(\theta,\omega) \tag{S7}$$

It evolves continuously to the normal state self-energy $\Sigma(\theta,\omega)$ above T_c where the distinction between $\Sigma_0(\theta,\omega)$ and $\Sigma_3(\theta,\omega)$ can not be made in the fitting process.

In this paper, we use the bare dispersion $\xi(\mathbf{k})$ given in Eqs. (3) and (11) in Ref. [25] with 6 parameters determined from very detailed fits to the band-structure calculated by density functional methods. We have also used the 4 parameters given in Ref. [17]. Although the measured Fermi-surfaces with the two band-structures are identical, the detailed dispersions differ at higher energies. The differences in the results using the two different band-structures are discussed as a source of systematic errors in **SII**.

SI.2 Procedure for Extracting the Self-Energy

The procedure we employ here is a combination of a refinement of the MDC fitting in Ref. [36] and a real frequency implementation of the MDC area ratio approach as proposed in Ref. [8] and [37]. The MDC self-energy analysis fits the ARPES intensity $I(\mathbf{k},\omega)$ of Eq. (S1) and (S2) for a fixed θ and ω with a chosen bare dispersion $\xi(\mathbf{k})$ as a function of $k_\perp$ to extract the $k_\perp$-independent normal self-energy $\Sigma(\theta,\omega)$ and pairing self-energy $\phi(\theta,\omega)$. The most important and unique feature of the MDC fitting is that one can determine the normal and pairing self-energies separately on an equal footing. One should notice the almost perfect MDC fittings shown in Figs. 2. This demonstrates the experimental justification of the $k_\perp$-independence of the self-energy and the matrix element $M(\mathbf{k},\nu)$ of Eq. (S1). The $k_\perp$-independence of M comes in

because the spectral function A of Eq. (S1) has a much sharper quasi-particle peak as a function of $k_\perp$ (at $k_\perp = k_m(\omega)$) than M. The $k_\perp$ dependence of $M(k_\perp)$ then can be factored out and written as a function of ω.

Now, the MDC area ratio approach takes the ratio of MDC areas in the superconducting and normal states, $\mathcal{A}_S(\theta,\omega)/\mathcal{A}_N(\theta,\omega)$, and equates it with the superconducting density of states.

$$ReN(\theta,\omega) = \frac{\mathcal{A}_S(\theta,\omega)}{\mathcal{A}_N(\theta,\omega)} = Re\left[\frac{\omega}{\sqrt{\omega^2 - \Delta^2(\theta,\omega)}}\right] \tag{S8}$$

This relation holds for general energy dependent DOS as well provided that the bandwidth is the largest energy scale. A combination of the two methods successfully produces the normal self-energy $\Sigma(\theta,\omega)$ and pairing self-energy $\phi(\theta,\omega)$.

The fitting of experimental MDC data $I(k_\perp,\theta,\omega)$ using Eq. (S1) in the normal state returns the $\Sigma(\theta,\omega)$ straightforwardly. In the superconducting state, however, it is a subtle matter because the fitting parameter space is expanded and yet, the parameters (the self-energies) must be determined by the small difference of the MDCs between the superconducting and normal states. Therefore the fitting must be aided by other information to ensure the reliable results. This is provided by the MDC area ratio approach.

The experimental results are taken along the trajectories shown in Fig. 2C, which are not straight lines in the $(k_\perp,\theta)$ plane, especially as the anti-nodal direction is approached. But the trajectories are known very well and one can convert from the points of measurement to $(k_\perp,\theta)$. It turns out that the corrections are significant only in $k_\perp$ compared to those in θ.

To calculate the area under the MDC, for the chosen θ, and a wide distribution of energies, by integrating the experimental $I(k_\perp,\theta,\omega)$ over $k_\perp$, the background $B(\mathbf{k},\omega)$ must first be subtracted. Over most of the energy range, $B(\mathbf{k},\omega)$ is independent of $k_\perp$ to a very good approximation, as seen in Fig. 2, and therefore can be easily determined. At higher energies,

above about 0.1 eV, it is weakly momentum dependent. The observed slight asymmetry of the MDC shape as a function of $k_\perp$ may be accounted for by a deviation of the bare dispersion $\xi(\mathbf{k})$ from the linear dispersion relation like the tight-binding dispersion or $k_\perp$ dependent background. We took the tight-binding dispersion for $\xi(\mathbf{k})$ and $k_\perp$-independent background, and proceed as follows.

(1) The initial calculation of the $ReN(\theta,\omega)$ begins with the MDC fittings with $\phi = 0$ for both $I_S(k_\perp,\theta,\omega)$ below T_c and $I_N(k_\perp,\theta,\omega)$ above T_c. This returns the backgrounds $B_S(\theta,\omega)$ and $B_N(\theta,\omega)$ as well as the normal self-energies. Then the MDC areas were calculated both in the superconducting and normal states after the backgrounds were subtracted off and used to calculate the superconducting DOS from Eq. (S8). This requires that the matrix element M of Eq. (S1) cancels out exactly in taking the ratio because the $k_\perp$ integral of the A gives the density of states. As discussed above, the matrix element M can be factored out of the $k_\perp$ integral of MDC area. Also, because M is independent of the temperature, it is cancelled out in taking the ratio.

(2) Take the Kramers-Kronig transform to obtain the imaginary part of $N(\theta,\omega)$. This gives a complete information on the complex function $N(\theta,\omega)$. The complex function $\Delta(\theta,\omega)$ is obtained from the relation,

$$\Delta(\theta,\omega) = \omega\left[1 - \frac{1}{N^2(\theta,\omega)}\right]^{\frac{1}{2}} \tag{S9}$$

The self-energies $\phi(\theta,\omega)$ are obtained from

$$\phi(\theta,\omega) = \Delta(\theta,\omega)Z(\theta,\omega) \tag{S10}$$

$$Z(\theta,\omega) = 1 - \frac{\Sigma(\theta,\omega)}{\omega} \tag{S11}$$

where $\Sigma(\theta,\omega)$ was already obtained as described in the step (1) above.

(3) Now, go back to the step (1) to make the MDC fittings of I_S and I_N, but allowing $\phi \neq 0$ below T_c. The predetermined Σ and ϕ in the step (2) serve as a guide to the subtle MDC fitting in the superconducting state. This returns improved Σ and ϕ as well as the background B.

(4) Go back to the step (2) to recalculate the MDC area with the newly determined background B. The resulting Σ and ϕ from Eq. (S10) and (S11) serve to make next iteration of MDC fittings. We iterate this process until the pairing self-energy from the MDC fitting and the MCD area ratio converge.

The self-energies presented here were obtained by the iterative process of the MDC fitting and MDC area ratio approach just explained.

A comment should be made here on the classic work of McMillan and Rowell[1]. They measured the ratio of the density of states in a tunneling conductance experiment on Pb as a function of energy in the superconducting state to that in the state just above T_c. This was used to obtain the gap function $\Delta(\omega)$ from which they deduced the Eliashberg function $\mathcal{E}_P$, (called $\alpha^2F(\omega)$ by them). This procedure works well for s-wave superconductors, where $\mathcal{E}_P = \mathcal{E}_N$, but this is not suitable for d-wave superconductors because $\mathcal{E}_P$ is in general different from $\mathcal{E}_N$. d-wave superconductivity requires two experimentally determined functions which may be determined from the coupled equations for the normal and the pairing self-energies to determine two distinct Eliahsberg functions $\mathcal{E}_N(\theta, \omega)$ and $\mathcal{E}_P(\theta, \omega)$ as is explained in **SIII**.

II. Correction of Systematic Errors and Renormalization of the ARPES Data

During the measurements, the sample orientation sometimes shows a small change with temperature, originating from the thermal expansion of the connection parts of the cryostat. This drift may induce a small angle (momentum) shift in the measured photoemission spectrum. This effect is too small to be removed in situ during the measurement by realigning the sample at each

temperature because of the limited motor-driven angular precision. For the high-precision data analysis performed in the present work which requires absolute measurements of counts of flux of electrons at the detector, such effects must be taken care of. We needed to carry out small intensity renormalization and angle shift corrections on the measured data. The corrections are based on the fact that, for ARPES data taken along a given momentum cut at different temperatures, the high binding energy part should show negligible change with temperature. In some of the measurements, no corrections are needed. This is illustrated in Fig. 1 in the main paper and especially the expanded panel C in it. In this case, the measurement condition is stable (negligible laser photon flux variation and negligible sample shift with temperature change), the high energy part stays the same for different temperatures in terms of both intensity and extracted dispersion (between -0.4 eV and -0.3 eV). Here no correction is necessary and MDCs are directly extracted. Fig. S1 illustrates a case in which corrections are needed. Momentum correction is performed to make sure that, at each temperature, the high energy dispersions coincide with each other by putting a small offset to the momentum along the cut direction. The coincidence of the high energy dispersions after such a correction in Fig. S1C, limited only by the noise in the data, validates the application of our momentum correction procedure.

The effect of the slight laser photon flux fluctuation on the data can be removed by normalizing the measured data at different temperatures so that the intensity of the high binding part is the same. Such an intensity normalization is performed as the first step in our data analysis.

Also important is to renormalize the MDCs in the superconducting state such that the pairing self-energy and accompanying deviation of the normal self-energy from above T_c is only determined by the difference in the ARPES intensities between the superconducting and normal states. Any misfits in the normal state may affect the superconducting state fittings and cause spurious results if done without the renormalization. The sources of the misfits in the normal state are most likely from the uncertainty of the bare dispersion as discussed below. The renormalizations were done as follows: We first fit the MDCs slightly above T_c, i.e., 97 K for UD89 data and 90 K for OD82 data, as a function of $k_\perp$ with the enforcement of $\phi = 0$ and

determine the normal state fitting curve. Then, we divide the MDC data to calculate the ratio, $I_S(k_\perp, \theta, \omega)/I_N(k_\perp, \theta, \omega)$, and multiply the ratio by the normal state fitting curve. This is the renormalized MDCs in the superconducting states we fit.

A significant source of the systematic error is the lack of precise knowledge of the bare dispersion $\xi(\mathbf{k})$ at high energies. The Fermi-surface is well fitted by more than one form of dispersion. As mentioned we have used two different parameterization of the band-structure. The results for normal self-energy near the Fermi-energy are always the same but differ far from it for ω larger than about $3\Delta \approx 65$ meV. However, we find very little variation in the pairing self-energy. This is because it is obtained from the differences of the data in the normal and superconducting states as discussed above, both of which are deduced with the same $\xi(\mathbf{k})$. The difference in the normal self-energy with the two different band-structures leads to differences which are discussed below.

The maximum entropy method for solution of integral equations can introduce unphysical oscillations in the results. These oscillations are uncontrollable in the solution of the integral equations if we take as input the raw deduced values of the self-energies, such as shown in Fig. 3. We average the measured self-energy at each energy over ± 5 meV around it as inputs to the integral equations. Even with such averaging, we obtain smoothly varying oscillatory results, varying at any energy by about $\pm 10\%$, through different constraints imposed in the process of the solution. We have guided ourselves by consistency and smooth variations of the results from one temperature to another. The final results presented for the Eliashberg functions are similar to the errors in the experiments discussed above. Adding all errors in quadrature, the results may be trusted only to about 10% at any energy up to about 0.1 eV and only up to about 15% at the maximum energies of about 0.2 eV.

SII.1 Limits of Validity of Results

Using a band-structure $\xi(\mathbf{k})$ given in high quality band-structure calculations, we can extract the absolute value of the normal self-energy $\Sigma(\mathbf{k}, \omega)$ to an accuracy of about 2% over the whole range of measurements and at all angles up to 0.45 eV. The poorest signal to noise ratio occurs in

determining the pairing self-energy $\phi(\mathbf{k},\omega)$ because it can only be extracted from the difference between the normal and superconducting state signals: $I_S(\mathbf{k},\omega) - I_N(\mathbf{k},\omega)$. It will be apparent below that the accuracy in extracting $\phi(\mathbf{k},\omega)$ is better than ~10% till up to ~0.2 eV for θ between 20° and 35° but progressively gets worse at larger energies; the data are not useful to directly deduce the pairing self-energy above about 0.2 eV. Similarly, signal to noise in ϕ becomes poorer when the momentum cuts come closer to the diagonal direction ($\theta = 45°$) and the temperature comes closer to T_c, because ϕ gets smaller. Therefore, such data were not used in the present analysis. It is expected that the next generation ARPES apparatus will be able to alleviate these limitations. However, it is expected that the principal conclusions of this paper, using the measured results and reasoned extrapolations from it, will continue to hold.

III. Equations for the Self-Energies

Eliashberg derived the integral equations for the normal and the pairing self-energies starting from a Hamiltonian of electrons and phonons through the leading order perturbation in the electron-phonon interactions. This is justified by the Migdal theorem and the small magnitude typically of the parameter $\lambda\omega_D/E_F$; λ is the dimensionless coupling constant, ω_D the Debye frequency, and E_F the typical band-width. In our case, the cut-off frequency of the fluctuations is similar to the band-width and the coupling constant is about 0.5. Therefore the accuracy of the extracted Eliashberg functions from the measured self-energies may be open to question. We first show here that, given an experimentally obtained self-energy function, the momentum and energy dependence of the collective modes leading to the self-energy can be determined from the Eliashberg equations without the Migdal or weak-coupling assumptions. This is true of the McMillan-Rowell type of results also. But in that case, Migdal's theorem obviates the need to pose the question. The procedure using the experimental self-energies to deduce the fluctuations, is quite different from calculating the self-energy using a spectra of fluctuations not obeying the Migdal approximation, which may be impossibly hard.

In the normal state, the self-energies can be expressed [38,39] exactly in terms of the irreducible vertex $\mathcal{I}(\mathbf{k},\mathbf{k}',\omega,\omega',\mathbf{q}=0,\Omega=0)$ and the exact Green's function $\hat{G}(\mathbf{k},\omega)$ of Eq. (3). This is

easily generalized to the superconducting state in which the relation between the self-energies, the vertices and the Green's function is shown in Fig. S2A. Assuming that the collective mode contributions to the vertex are a function primarily of the energy transfer $(\omega - \omega')$, the integral Eq. S2A for the self-energy is,

$$\hat{\Sigma}(\mathbf{k},\omega) = \int d\omega' Tr \sum_{k'} \mathcal{I}(\mathbf{k},\mathbf{k}',\omega-\omega',\mathbf{q}=0,\Omega=0)\hat{G}(\mathbf{k}',\omega') \tag{S12}$$

This equation is in the Gorkov-Nambu space,

$$\hat{\Sigma}(\mathbf{k},\omega) \equiv \Sigma_0(\mathbf{k},\omega)\tau_0 + \Sigma_3(\mathbf{k},\omega)\tau_3 + \phi(\mathbf{k},\omega)\tau_1 \tag{S13}$$

Similarly $\hat{G}(\mathbf{k},\omega)$ is given in τ-space as in Eq. (S3). $\mathcal{I}$ is similarly the sum of the normal $\tau_3\tau_3$ part, $\mathcal{I}_{33}$, and a $\tau_1\tau_1$ part $\mathcal{I}_{11}$. The trace in Eq. (S12) is in τ-space. $\mathcal{I}$ is irreducible in the $(\mathbf{q},\Omega)$ particle-hole channel. Further, $\mathcal{I} = \mathcal{I}^{(0)} + \mathcal{I}^{(1)}$, the sum of a part with total spin 0 and with 1. Given the correct $\hat{\Sigma}(\mathbf{k},\omega)$, the solution of this integral equation gives the equally correct irreducible vertex $\mathcal{I}(\mathbf{k},\mathbf{k}',\omega,\omega')$. Since Eq. (S12) is exact, it includes all vertex corrections and self-energy insertions in a perturbative calculation of the self-energy.

One may further write, for a square lattice with s or d-wave pairing,

$$\mathcal{I}_{33}(\mathbf{k},\mathbf{k}',\nu) = g_0 A_{1g}(\hat{k}) A_{1g}(\hat{k}') I_{33}(k,k',\nu) + \tag{S14}$$

$$\begin{aligned}\mathcal{I}_{11}(\mathbf{k},\mathbf{k}',\nu) = {} & g_{2,1} B_{1g}(\hat{k}) B_{1g}(\hat{k}') I_{11}(k,k',\nu) \\ & + g_{2,2} B_{2g}(\hat{k}) B_{2g}(\hat{k}') I_{11}(k,k',\nu) +\end{aligned} \tag{S15}$$

where $A_{1g}, B_{1g}, B_{2g}, ..$ are the relevant irreducible representations of the point group and the g's are the corresponding coupling constants.

Since the normal self-energy must be of A_{1g} symmetry and superconductivity in cuprates is in

B_{1g} symmetry, it follows from Eq. (S12) that measurement of the normal and pairing self-energy and the solution of that equation yields, on integration over $\mathbf{k}'$, (using symmetry of the vertices under interchange of k and k'), the irreducible vertices in the normal $I_{33}(k,k',\nu)$ and the pairing $I_{11}(k,k',\nu)$ channels. Eqs. (S12, vertex-decomp) are shown below to be identical to the more familar Eliashberg equations.

SIII.2 Familar Eliashberg Integral Equations for d-wave Superconductors

If as assumed above, the dependence of the irreducible vertex on ω and ω' is only through the energy transfer $(\omega-\omega')$, Fig. S2A are identical to the more familiar skeleton diagrams for the self-energy, shown as Fig. S2B. To show this, we identify that the irreducible vertex for the normal self-energy $\mathcal{I}_{33}(\mathbf{k},\mathbf{k}',\nu)=g(\hat{k},\hat{k'})F(\mathbf{k},\mathbf{k}',\nu)g(\hat{k'},\hat{k})$, and for the pairing self-energy $\mathcal{I}_{11}(\mathbf{k},\mathbf{k}',\nu)=g(\hat{k},\hat{k'})F(\mathbf{k},\mathbf{k}',\nu)g(-\hat{k},-\hat{k'})$. Now consider Eq. (S12). On re-expressing $G(\mathbf{k},\omega)$ in terms of the spectral function and re-arranging, the familiar Eliashberg equations [2,3] (S16-S17) below, as generalized for d-wave superconductivity[27,13], follow in terms of the normal Eliashberg function $\mathcal{E}_N(\theta,\omega)$ and the d-wave pairing Eliashberg function $\mathcal{E}_P(\theta,\omega)$, defined below.

$$\Sigma(\theta,\omega)=\int_{-\infty}^{\infty}d\omega' L(\omega,\omega')\mathcal{E}_N(\theta,\omega') \tag{S16}$$

$$\phi(\theta,\omega)=-\int_{-\infty}^{\infty}d\omega' M(\omega,\omega')\mathcal{E}_P(\theta,\omega') \tag{S17}$$

$$L(\omega,\omega')\equiv\int_{-\infty}^{\infty}\frac{f(\varepsilon)+n(-\omega')}{\varepsilon+\omega'-\omega-i\delta}N_1(\varepsilon) \tag{S18}$$

$$M(\omega,\omega')\equiv\int_{-\infty}^{\infty}\frac{f(\varepsilon)+n(-\omega')}{\varepsilon+\omega'-\omega-i\delta}D_1(\varepsilon) \tag{S19}$$

$$N_1(\varepsilon) \equiv < Re \frac{W(\theta', \varepsilon)}{\sqrt{W^2(\theta', \varepsilon) - \phi^2(\theta', \varepsilon)}} >_{\theta'} \tag{S20}$$

$$D_1(\varepsilon) \equiv < Re \frac{2\,\phi(\theta', \varepsilon)\cos(2\theta')}{\sqrt{W^2(\theta', \varepsilon) - \phi^2(\theta', \varepsilon)}} >_{\theta'} \tag{S21}$$

Here $<..>_{\theta'}$ implies the normalized integral over θ'. The normal and pairing Eliashberg functions are given in terms of the coupling constant and interaction vertices,

$$N_1(\varepsilon)\mathcal{E}_N(\mathbf{k}, \omega) = \int d\mathbf{k}' A_N(\mathbf{k}', \varepsilon)[|g^{(0)}(\mathbf{k}, \mathbf{k}')|^2(-\frac{1}{\pi})Im\mathcal{F}^{(0)}(\mathbf{k}, \mathbf{k}', \omega) + 3\left|g^{(1)}(\mathbf{k}, \mathbf{k}')|^2\left(-\frac{1}{\pi}\right)ImF^{(1)}(\mathbf{k}, \mathbf{k}', \omega)\right] \tag{S22}$$

$$D_1(\varepsilon)\mathcal{E}_P(\mathbf{k}, \omega) = \int d\mathbf{k}' A_\phi(\mathbf{k}', \varepsilon)[g^{(0)}(\mathbf{k}, \mathbf{k}')g^{(0)}(-\mathbf{k}, -\mathbf{k}')(-\frac{1}{\pi})Im\mathcal{F}^{(0)}(\mathbf{k}, \mathbf{k}', \omega) - 3g^{(1)}(\mathbf{k}, \mathbf{k}')g^{(1)}(-\mathbf{k}, -\mathbf{k}')(-\frac{1}{\pi})ImF^{(1)}(\mathbf{k}, \mathbf{k}', \omega)] \tag{S23}$$

$F^{(0)}(\mathbf{k}, \mathbf{k}', \omega)$ and $F^{(1)}(\mathbf{k}, \mathbf{k}', \omega)$ are, respectively, the spin-0 and spin-1 fluctuation propagators. Their corresponding vertices with fermions are $g^{(0)}(\mathbf{k}, \mathbf{k}')$ and $g^{(1)}(\mathbf{k}, \mathbf{k}')$ respectively. A and A_ϕ are, respectively, the normal single-particle spectral function of Eq. (S2) and the pairing part (12 component in τ-space) of the matrix single-particle spectral function given in terms of Eq. (S3). $A(\mathbf{k}, \omega)$ has the full symmetry of the lattice $A_{1g}(\hat{k})$. And $A_\phi(\mathbf{k}, \omega)$ has the angular dependence $B_{1g}(\hat{k})$. In the isotropic approximation, the angle-dependences are 1 and $\sqrt{2}\cos(2\theta)$, respectively.

Eqs. (S16 – S23) are used to solve for the Eliashberg functions. We first calculate N_1 and D_1 from Eq. (S20) using the self-energies extracted from the fits to MDCs, and then calculate the matrices M and L from Eq. (S18 – S19). The inverse matrices of L and M are used to obtain $\mathcal{E}_N$ from Σ and $\mathcal{E}_P$ from ϕ. The inversion matrices L^{-1} and M^{-1} were calculated using the

maximum entropy method to treat the logarithmically singular cases as well.

IV. Comparison of theories with the results from experiments

We now consider some of the ideas and calculations for models of cuprates in relation to the Eliashberg theory and the experimental results presented in the main paper.

Phonons

The only part of the effective interactions deduced by the experiments in the characteristic energy range of the phonons is the broad feature around 50 meV. But this is absent in the pairing Eliashberg function $\mathcal{E}_P$ in the d-wave channel near T_c. As generally agreed, phonons are not responsible for d-wave pairing in the cuprates.

Antiferromagnetic Fluctuations

In the usual theory[22,40] of promotion of d-wave superconductivity by antiferromagnetic (AFM) fluctuations, $g^{(1)}(\mathbf{k},\mathbf{k}')g^{(1)}(-\mathbf{k},-\mathbf{k}') = |g^{(1)}(\mathbf{k},\mathbf{k}')|^2$. The spin-1 fluctuations $\mathcal{F}^{(1)}(\mathbf{k},\mathbf{k}',\omega)$, projected to the B_{1g} channel leads to a sign for $\mathcal{E}_P$ which is opposite to that projected to identity. d-wave superconductivity is therefore expected. The AFM fluctuations of the Hubbard model do provide an attractive pairing in the d-wave channel if their correlation length is much larger[22,40,41] than k_F^{-1}.

Systematic calculations[28] have used the measured q-dependent spin-fluctuation spectra[29] in $La_{2-x}Sr_xCuO_4$ at various x in the Eliashberg equations to calculate the momentum and frequency dependence of the normal and pairing self-energies, $\Sigma(\mathbf{k},\omega)$ and $\phi(\mathbf{k},\omega)$. The unknown coupling constant is adjusted to give the measured values of T_c. This coupling constant has to be adjusted upwards with increased doping because the amplitude of the fluctuations go down with doping in the measurements while T_c goes up. The calculated results for the pairing self-energy near optimal doping at various angles are shown in Fig. S3. The angle dependence shows the B_{1g} dependence of the d-wave gap, but the frequency dependence is strongly peaked (with some structure in between) in the low energy region at about 0.1 eV and then goes to 0 rapidly. The

physics of the peak and the reason for the rapid vanishing of the self-energy are fully discussed in Ref. [28] in terms of the measured antiferromagnetic fluctuations. The dependence in Fig. S3 should be compared with the experimental results for the pairing self-energy shown in Fig. 3, where a nearly constant dependence is found up to the cut-off, beside the superconductivity induced low energy features. Similar results with peaking of the pairing self-energy at lower energy, consistent with a longer AFM correlation length, appear in the calculated results Ref. [28] on using the data at lower dopings. The calculated normal self-energy $\Sigma(\theta,\omega)$ (See Figs. (2-4) of Ref. [28]) shows a strong θ dependence and does not have a linear in ω dependence. Since the normal self-energy in these calculations is angle dependent, ideas based on such calculations cannot be used to address the "central paradox" – that the normal self-energy is angle independent while the pairing is in the d-wave channel.

Fluctuations of the Hubbard Model

A very sophisticated calculation of the normal self-energy and the gap $\Delta(\omega)$ starting with the one band Hubbard model, using 8 site cluster dynamical mean-field theory at various dopings has been performed[30]. Such calculations do not provide the angle dependence of the self-energy and one must assume, quite reasonably, that it is in the d-wave channel just like the experiments. In other calculations on the same model with variants of the same technique[42], d-wave superconductivity is found. We show in Fig. S4 the frequency dependence of the gap $Im\Delta(\omega)$. These are also peaked at low energies, at about 0.2 and 1 in units of the kinetic energy parameter t, with nearly 0 in between. The parameter t is adjusted in these calculations to be about 0.3 eV because the maximum T_c as a function of doping in the calculations is $\approx t/60$. The normal self-energy has also been calculated, for example Fig. (5) in Ref. [31]. The normal self-energy is constant beyond about $0.2\ t$. The calculated results should be compared with the experimental results in Fig. 3.

Fluctuations of Loop-Current Order

The motivation of this model comes from the observation of diffraction pattern with polarized elastic neutron scattering[43] consistent with loop-current order[44,45] in four different families of underdoped cuprates, with a quantum-critical point near optimal doping. The quantum-critical

fluctuations of the loop-current model belong to the universality class of the dissipative quantum XY model. Over a range of parameters, they have been derived[46,47] and checked and extended by Monte-Carlo calculations[32.] Such fluctuations provide $\mathcal{F}_0(\mathbf{k},\mathbf{k}',\omega)$ with a scale-invariant frequency dependence $\propto \tanh(\omega/2T)$ in the normal state up to a cut-off ω_c. This frequency dependence is consistent with the frequency dependence of $\mathcal{F}_0(\omega)$ deduced above from $\mathcal{E}_N$ for $T \gtrsim T_c$, except for the 50 meV bump, and $\mathcal{E}_P$ for $T \to T_c$, as well as for the normal state singular-Fermi-liquid properties[48]. This form of $\mathcal{F}_0(\mathbf{k},\mathbf{k}',\omega)$ leads to frequency dependence observed in the experimental normal and pairing self-energies. Evidence of the latter is the calculation and comparison with the pairing self-energy starting from the measured $\mathcal{E}_N(\omega) \approx \mathcal{E}_P(\theta,\omega)/\cos(2\theta)$ near T_c, given in Fig. 5.

From the point of the experimental results in this paper, a crucial aspect of such fluctuations is that they resolve the central paradox of the high T_c problem in cuprates, that the normal self-energy is nearly angle-independent and the pairing is in the d-wave channel. To see this, one must consider the vertex $g(\mathbf{k},\mathbf{k}')$ for such fluctuations to fermions. It has been derived[33] that scattering of fermions occurs with such fluctuations through their angular momentum. For an isotropic approximation to the fermion dispersion near the Fermi-surface (results with lattice symmetry have been given in Ref. [33] but within the accuracy of the results obtained here, the isotropic approximation is adequate),

$$g(\mathbf{k},\mathbf{k}') = i g_0\left(\hat{\mathbf{k}} \times \hat{\mathbf{k}}'\right) \tag{S24}$$

The angle-dependence in $\Sigma(\theta,\omega)$ and $\phi(\theta,\omega)$ comes from integrating the vertex part of the effective interactions,

$$|g(\mathbf{k},\mathbf{k}')|^2 = -g(\mathbf{k},\mathbf{k}')g(-\mathbf{k},-\mathbf{k}') = \frac{g_0^2}{2}[1-(\cos2\theta\cos2\theta' + \sin2\theta\sin2\theta')] \tag{S25}$$

over $\mathbf{k}'$ projected over the intermediate Green's function shown in Fig. (S2) A and B respectively. The intermediate state has the full symmetry of the lattice; only the first term in Eq.

(S25) then contributes on integration over θ'. One therefore finds that $\Sigma(\mathbf{k},\omega)$ is only a function of ω.

Now, consider $\phi(\theta,\omega)$. Since the intermediate state at θ' is $\propto \cos(2\theta')$, only the second term in Eq. (S25) contributes on integration over θ', so that $\phi(\theta,\omega) \propto \cos(2\theta)$. Note that this part of the vertex is attractive while the s-wave part is repulsive in the pairing channel. The central paradox of high temperature superconductivity in cuprates is thus resolved. This has required $\mathcal{F}$ to be nearly momentum-independent or equivalently be a separable function of momentum transfer and energy, as in the criticality derived for the observed order. The result that $\tilde{\mathcal{E}}_P(\omega) \approx \mathcal{E}_N(\omega)$ also follows. Corrections due to lattice symmetry may actually be expected in their ratio but not in the frequency dependence. In the isotropic approximation, the two *attractive* d-wave channels in 2D in Eq. (S25) give degenerate results. But, in the cuprates, the density of states projected to $\cos(2\theta)$ or $d_{x^2-y^2}$ symmetry is larger than that in $\sin(2\theta)$ or d_{xy}-symmetry favoring the former. The central paradox as to how the normal self-energy is angle-independent but the pairing self-energy has $\cos(2\theta)$ dependence is therefor resolved if the primary interaction among the fermions is through exchange of quantum critical fluctuations of the loop current order with a vertex with the symmetry of Eq. (S24).

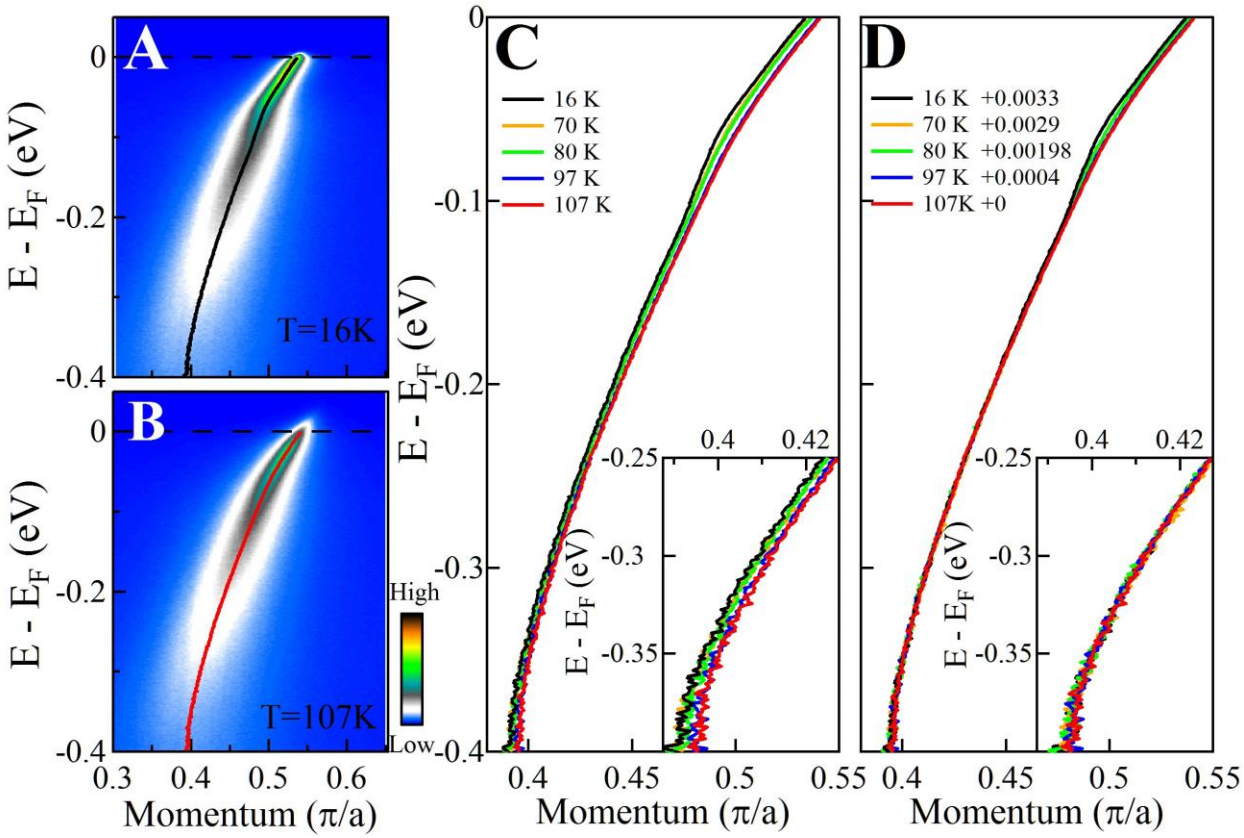

FIG. S1: **Illustration of corrections to data needed due to systematic errors due to movement of sample with change in temperature**. Color representation of the measured photoemission intensity along 10° to the Brillouin Zone in UD89 sample. (a) at 107 K and (b) at 16 K. (c) gives the progression of the Energy-momentum dispersions at temperatures 16 K, 70 K, 80 K, 97 K and 107 K. The inset in (c) gives on an expanded scale the illustration of the errors in the data due to sample movement on an expanded scale. In (d) and its inset, we show how we correct the systematic errors by aligning the high energy parts at different temperatures. The error in the raw data shown is the maximum in the data that we chose to analyze.

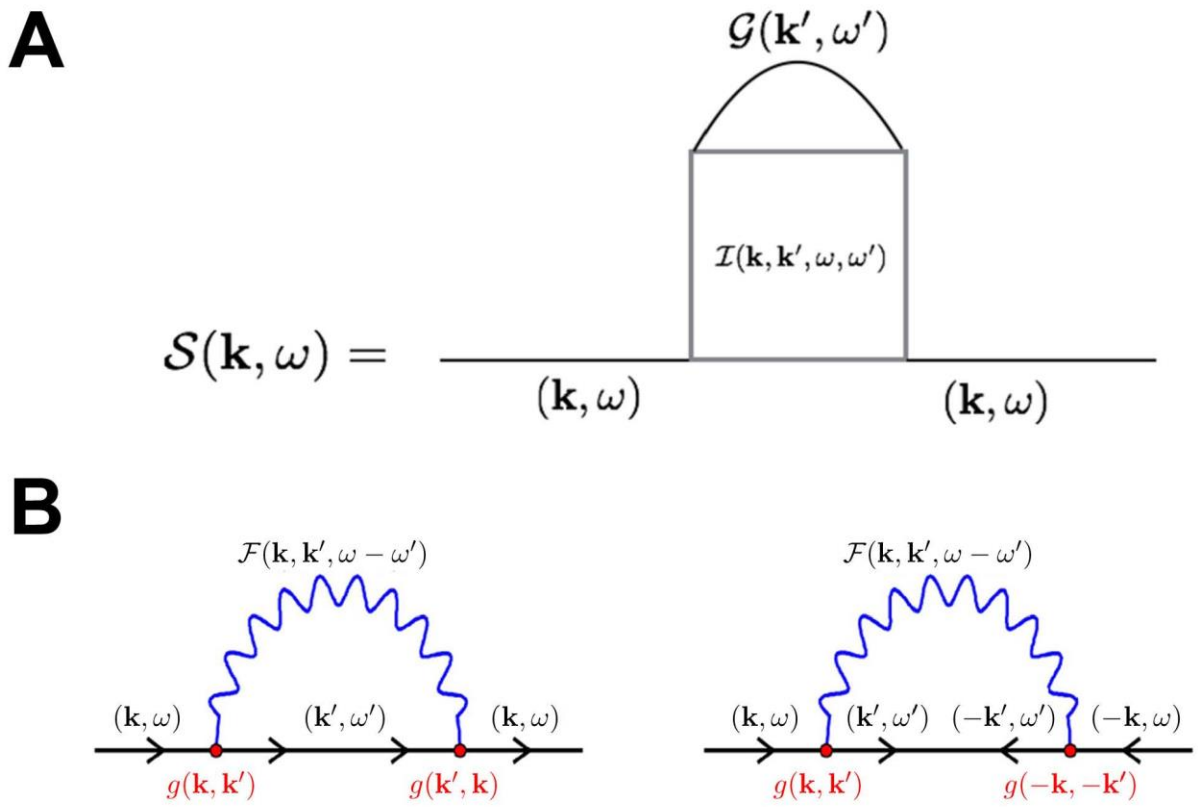

FIG. S2: **Exact representation of the normal and pairing self-energies**. **A** gives the self-energy in Gor'kov-Nambu space in terms of the exact Irreducible vertex and the exact Green's function. **B** is equivalent to **A** in terms of the more familiar skeleton diagrams, and gives on the left the the normal self-energy $\Sigma(\mathbf{k}, \omega)$ and on the right the pairing self-energy $\phi(\mathbf{k}, \omega)$. The direction of the external legs of the vertex $\mathcal{I}$, of the self-energy S, and of the Green's function $\mathcal{G}$ in **A** for the normal and the pairing self-energy components are identical to those in **B**. The wiggly line in **B** are the fluctuations $F(\mathbf{k}, \mathbf{k}', \omega - \omega')$ exchanged by the fermions through vertices $g(\mathbf{k}, \mathbf{k}')$. The normal self-energy as a function of $(\mathbf{k})$ as well as the intermediate normal state propagator on the left as a function of $(\mathbf{k}')$ have the full symmetry of the lattice, while on the right, the intermediate pairing propagator at $\mathbf{k}', -\mathbf{k}'$ as well as the pairing self-energy at $\mathbf{k}, -\mathbf{k}$ have the symmetry of d-wave superconductivity; for example, the latter transforms as $\cos 2\theta_{\hat{\mathbf{k}}}$ in the continuum approximation.

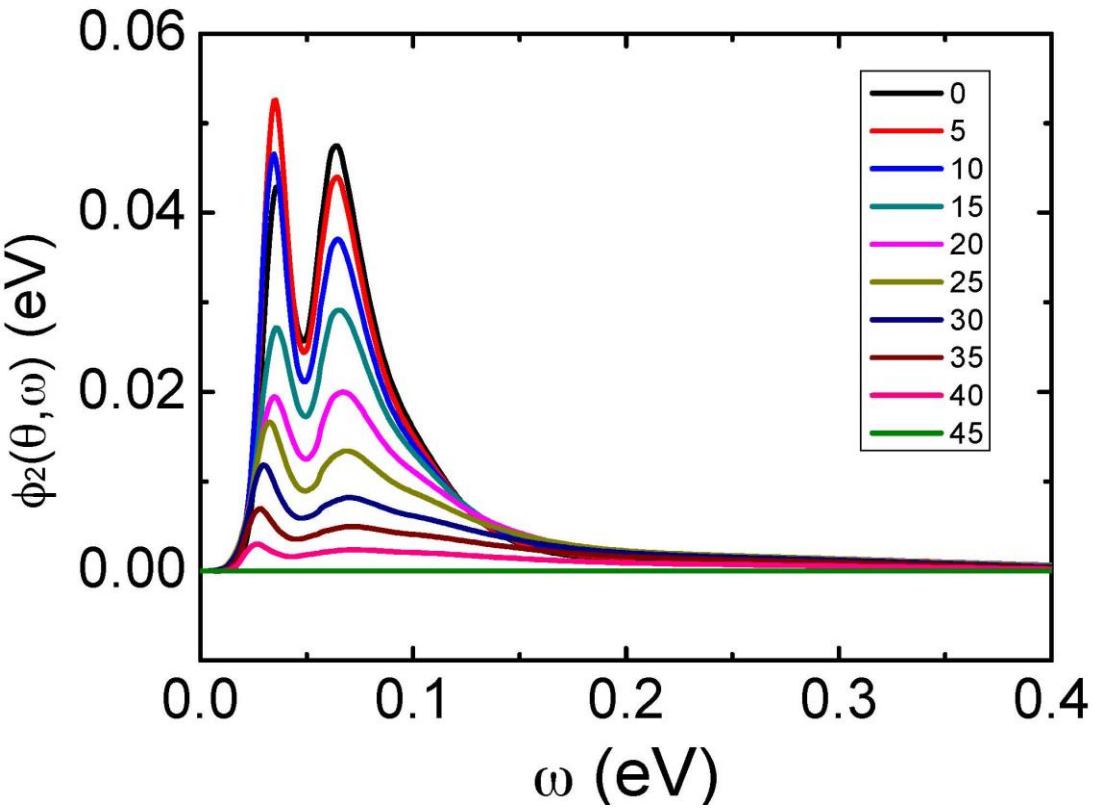

FIG. S3: **The Imaginary part of the pairing self-energy** at various angles across the Fermi-surface calculated in Ref. [28] from the measured spin-fluctuation spectra in $La_{2-x}Sr_xCuO_4$ by Vignolle et al. Ref. [29] at optimal doping. Results at other dopings may be read in the references given as also the calculated normal self-energy. The frequency dependence calculated does not compare well with the experimental pairing self-energy in Fig. 3, although its angular dependence is consistent with d-wave superconductivity.

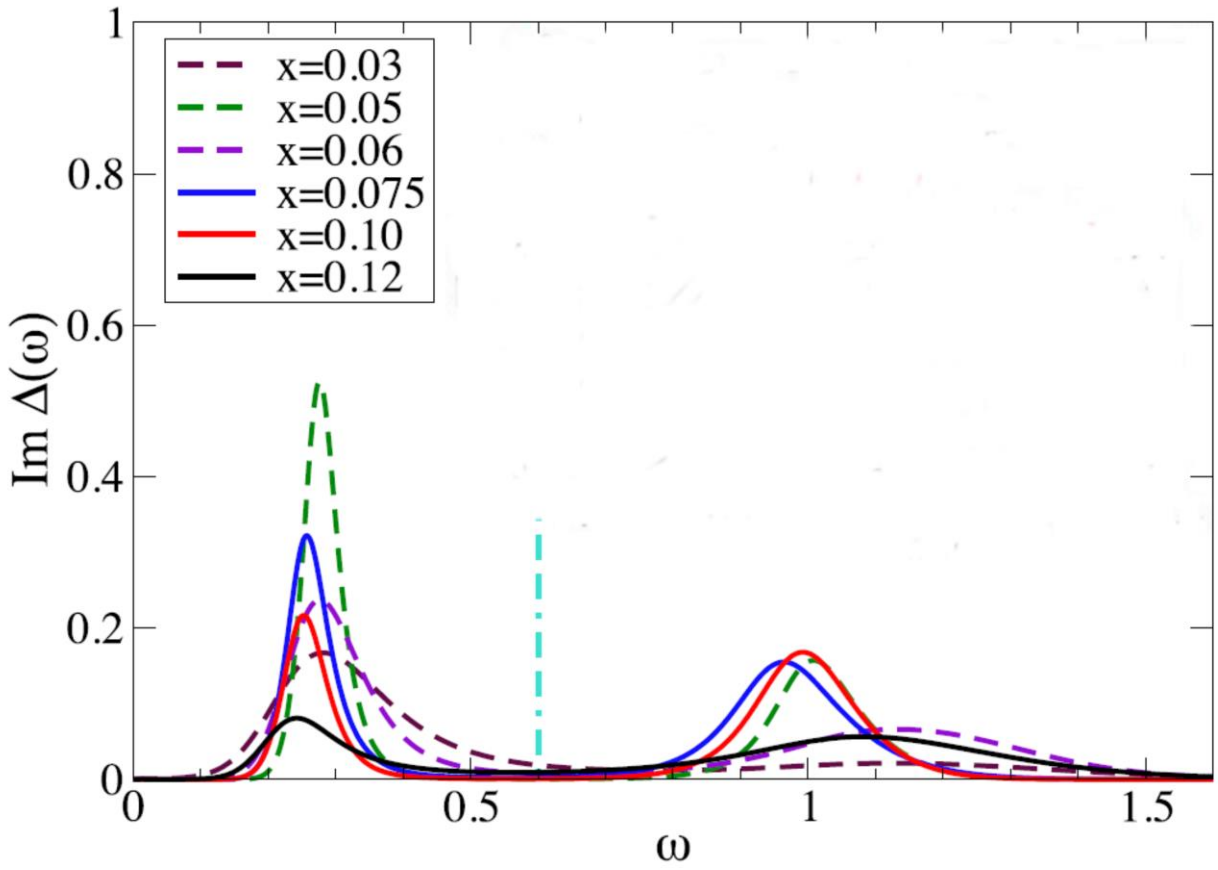

FIG. S4: **Imaginary part of the gap function for the Hubbard model** calculated by Ref. [30] for various dopings indicated in the plot. (The vertical dashed line is used for some other purposes in this reference and does not concern us.) The energy scale ω is in units of the kinetic energy parameter $t \approx 0.3eV$, chosen to get the maximum T_c as a function of doping to be $t/60$, and the local repulsion parameter $U = 6t$. The gap function $\Delta(\omega)$ and the pairing self-energy $\phi(\omega)$ are related by the quasi-particle renormalization $Z(\omega)$, which is very weakly ω-dependent. The result shown here, specifically the rapid decrease to nearly 0 between the two bumps, does not compare well with the frequency dependence of the experimental pairing self-energy in Fig. 3.